Supplementary Information for Two-Step Heat Fusion Kinetics and Mechanical Performance of Thermoplastic Interfaces

Shijun Wang[1,4], **Jiaxin Shi**[2], **Takayuki Shimizu**[3,*], **Jun Xu**[2,*], **and Zhiping Xu**[1,*]

[1]Applied Mechanics Laboratory, Department of Engineering Mechanics and Center for Nano and Micro Mechanics, Tsinghua University, Beijing, 100084, China
[2]Department of Chemical Engineering, Tsinghua University, Beijing, 100084, China
[3]Strength Research Department, Research & Innovation Center, Mitsubishi Heavy Industries Ltd., Japan
[4]National Center for Nanoscience and Technology, Beijing, 100190, China
[*]Correspondence and requests for materials should be addressed to T. Shimizu (takayuki.shimizu.s2@mhi.com), J. Xu (jun-xu@tsinghua.edu.cn), Z. Xu (xuzp@tsinghua.edu.cn)

Supporting Information Available

This Supplementary Information Material includes **Supplementary Figures S1-S10**.

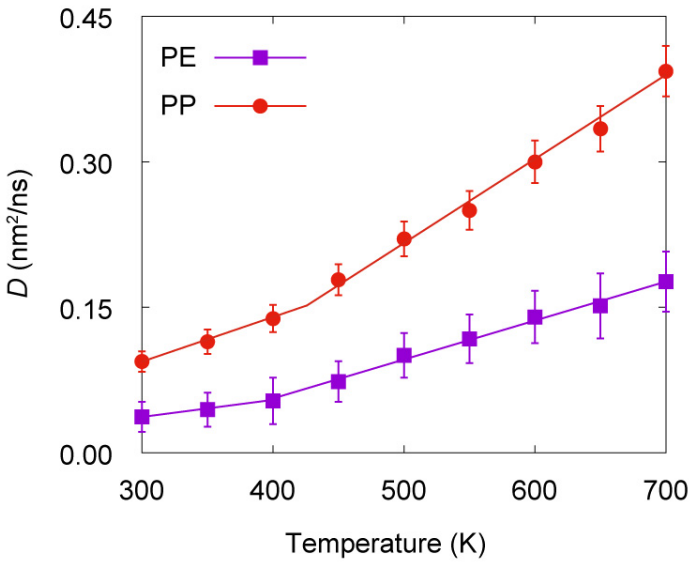

Figure S1. Coefficients of diffusion, *D*, plotted as functions of temperature for PE and PP as predicted by coarse-grained molecular dynamics (CGMD) simulations. The length (*n*100) indicates 100 beads of PE and 130 beads of PP in the CG model. The pressure is 1 atm.

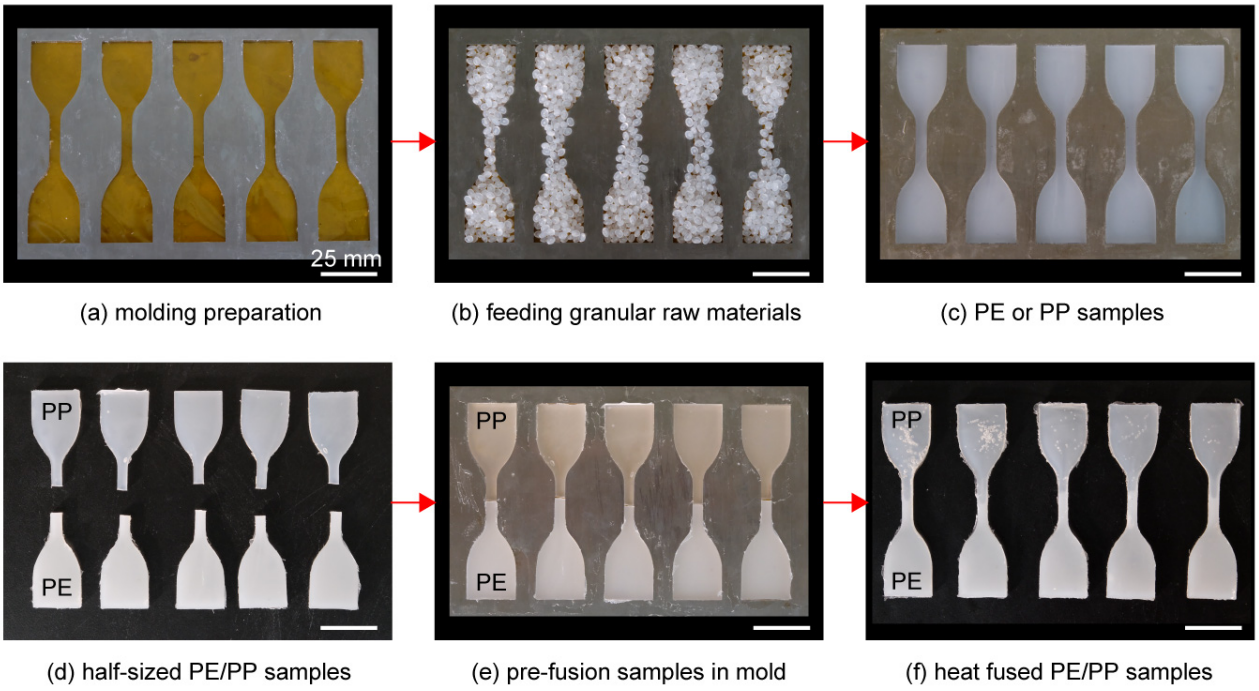

Figure S2. Flow charts of hot-compression molding (HCM) employed to manufacture fused PE/PP samples.

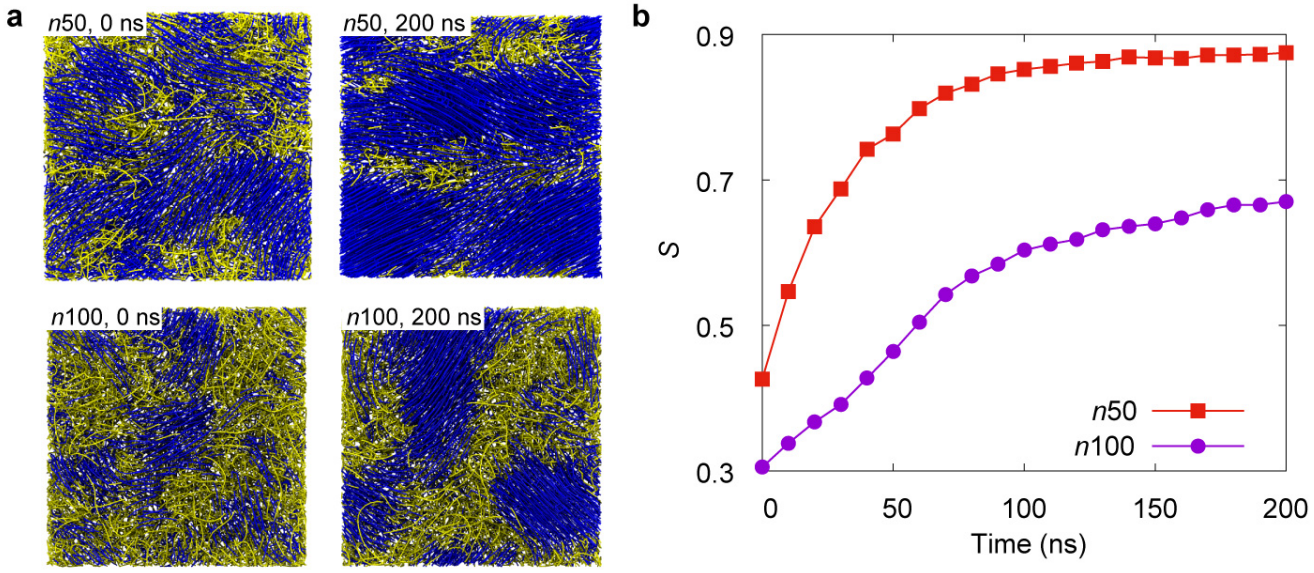

Figure S3. (**a**) Microstructural evolution of PE chains obtained from CG simulations. The ordered region $(s_i > 0.7)$ is highlighted in blue color, and amorphous region $(s_i < 0.7)$ in yellow. (**b**) Self-arrangement of PE chains characterized by the order parameter $S \in [0, 1]$ as a function of fusion time, where the chain length is chosen according to the $n50$ and $n100$ models. Higher values of S indicate more ordered structures.

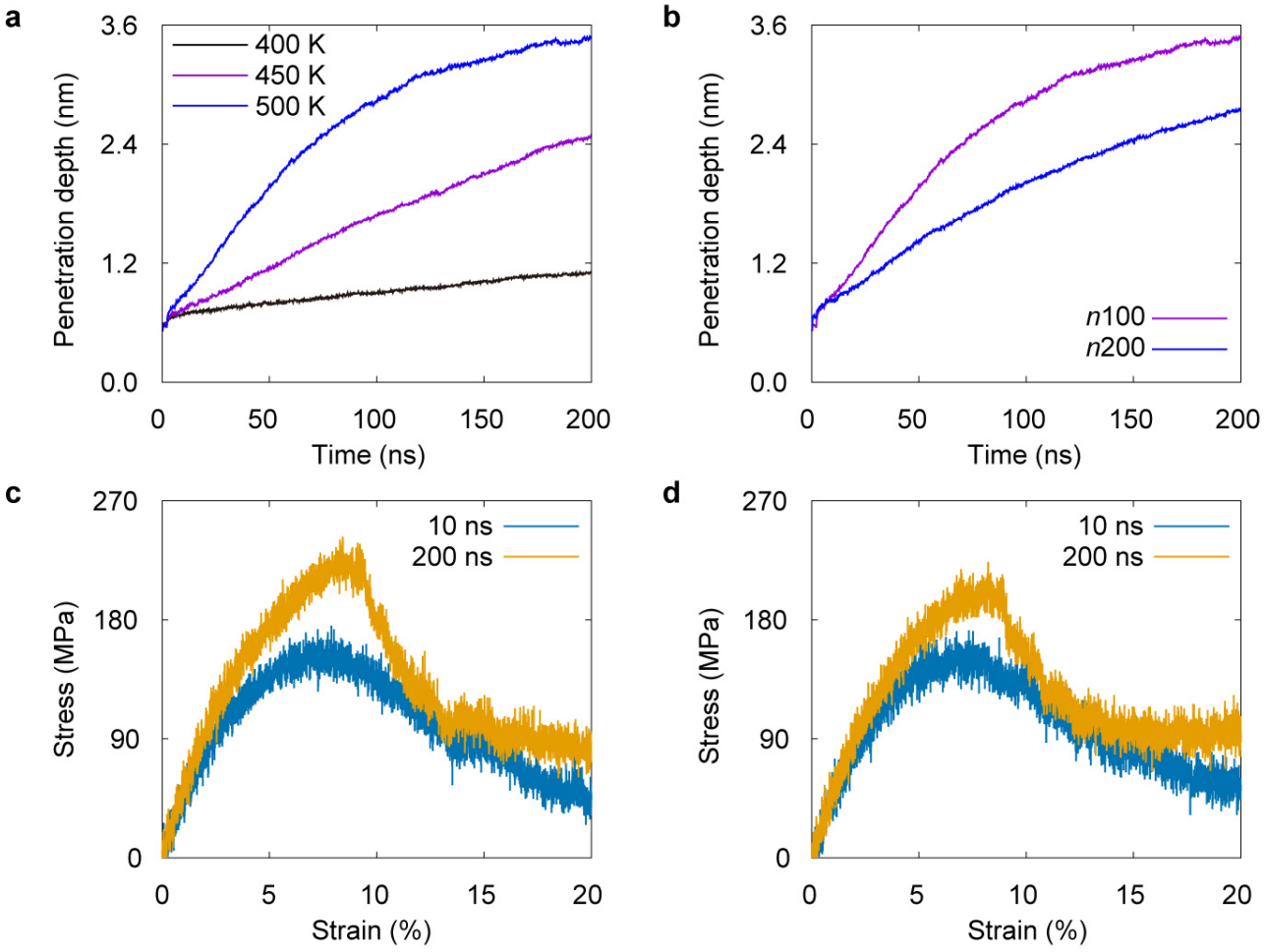

Figure S4. Penetration depth of the PE/PP interfaces at different (**a**) fusion temperature ($T = 400, 450, 500$ K) and (**b**) chain lengths ($n100$ and $n200$). Stress-strain curves for the samples with chain lengths (**c**) $n100$ and (**d**) $n200$, where the time of fusion is 10 and 200 ns.

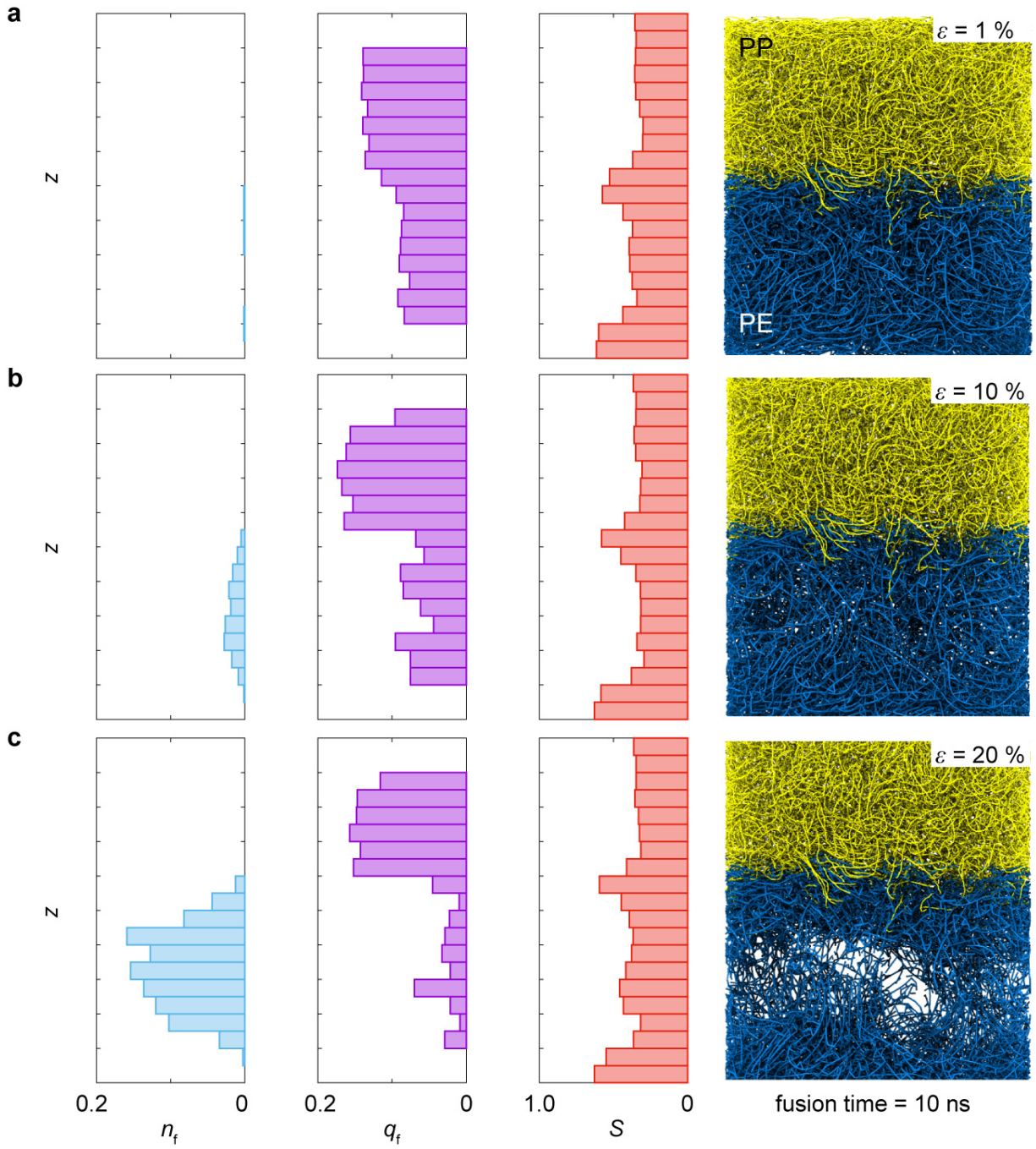

Figure S5. Microstructural evolution of the PE/PP interfaces under tensile strain of (**a**) $\varepsilon = 1\%$, (**b**) 10%, (**c**) 20%. The three columns are the spatial distributions, in the direction normal to the interface, of the fraction of fractured bonds n_f, the load filling factor q_f, and the order parameter S from the left to the right. The PE/PP interface is fused for 10 ns, at 500 K and 1 atm.

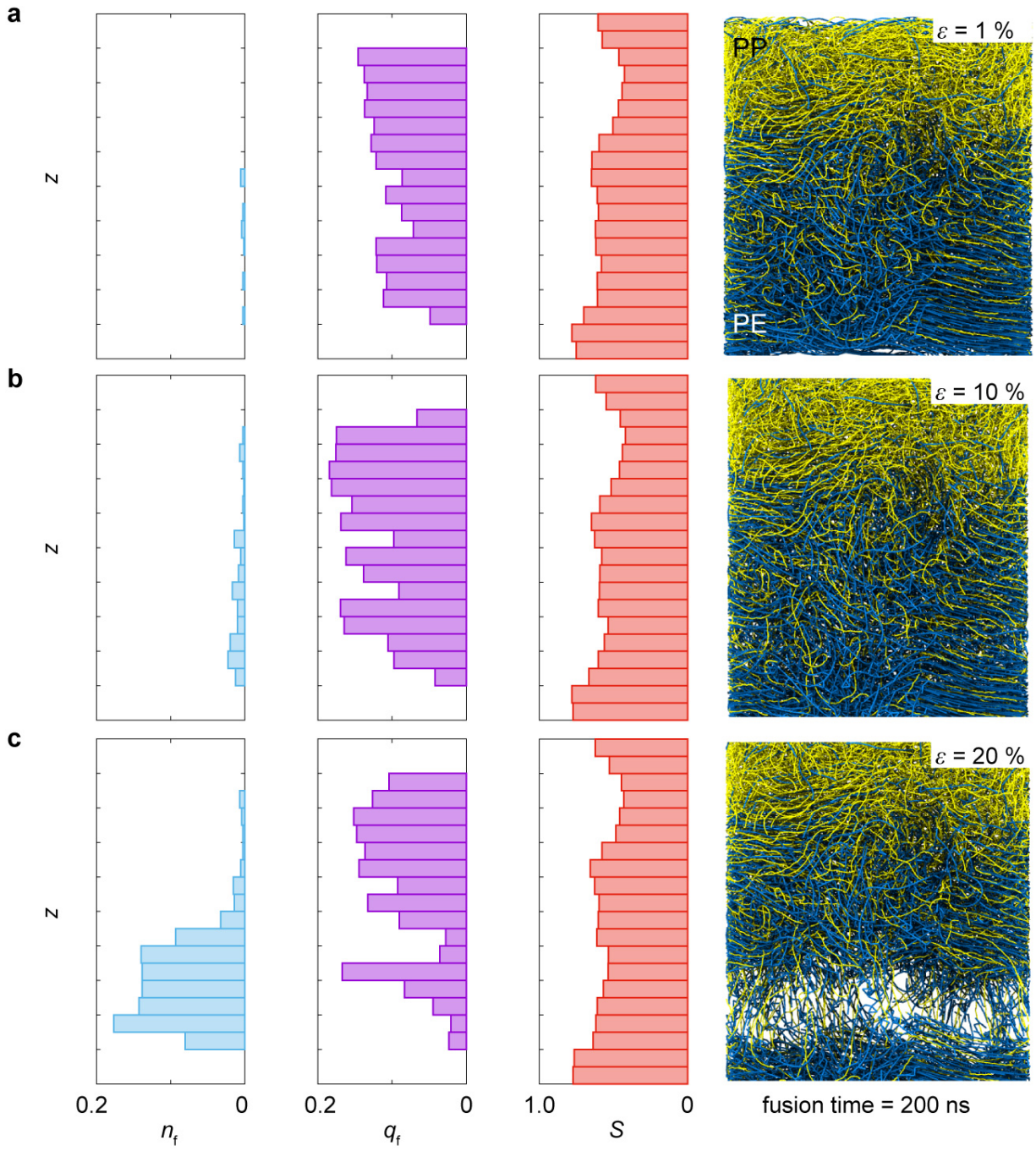

Figure S6. Microstructural evolution of the PE/PP interfaces under tensile strain of (**a**) $\varepsilon = 1\%$, (**b**) 10%, (**c**) 20%. The three columns are the spatial distributions, in the direction normal to the interface, of the fraction of fractured bonds n_f, the load filling factor q_f, and the order parameter S from the left to the right. The PE/PP interface is fused for 200 ns, at 500 K and 1 atm.

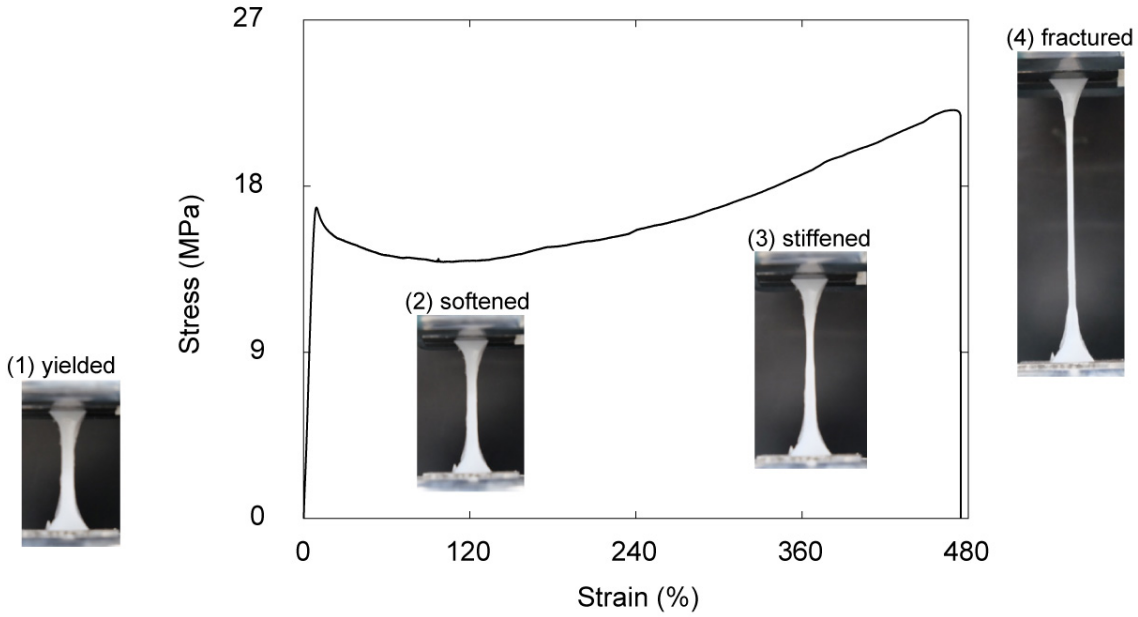

Figure S7. A typical stress-strain curve of the pure PP-2 sample.

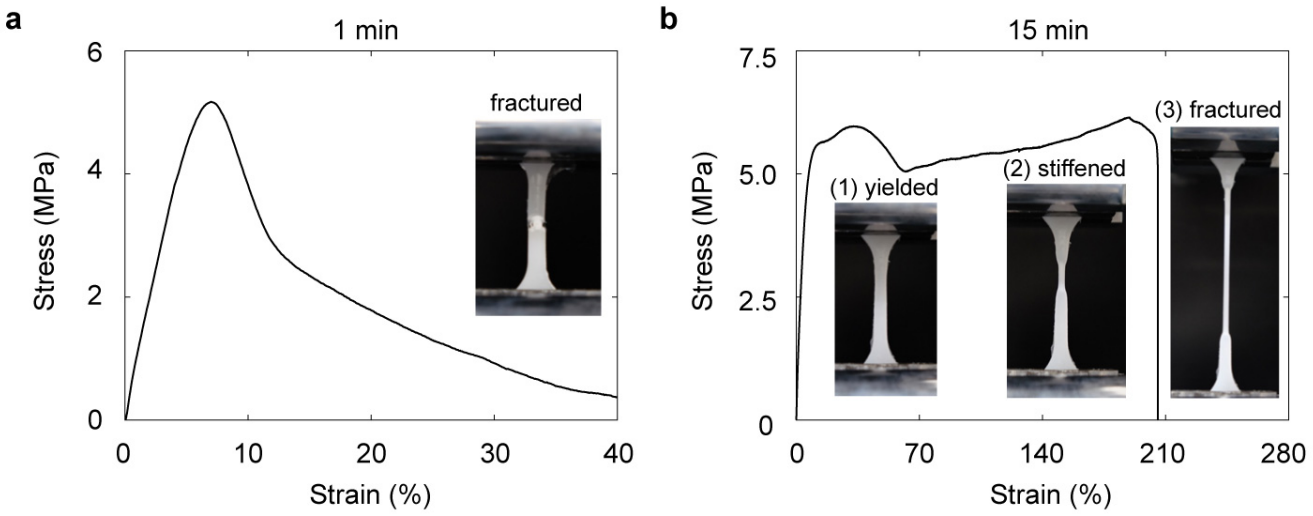

Figure S8. Stress-strain curves for the fused LLDPE/PP-1 samples obtained with (**a**) shorter (1 min) and (**b**) longer fusion time (15 min). The fusion temperature is 180 °C. As the time of fusion increases, the interface is strong and thus the strength is dominated by the part of bulk LLDPE.

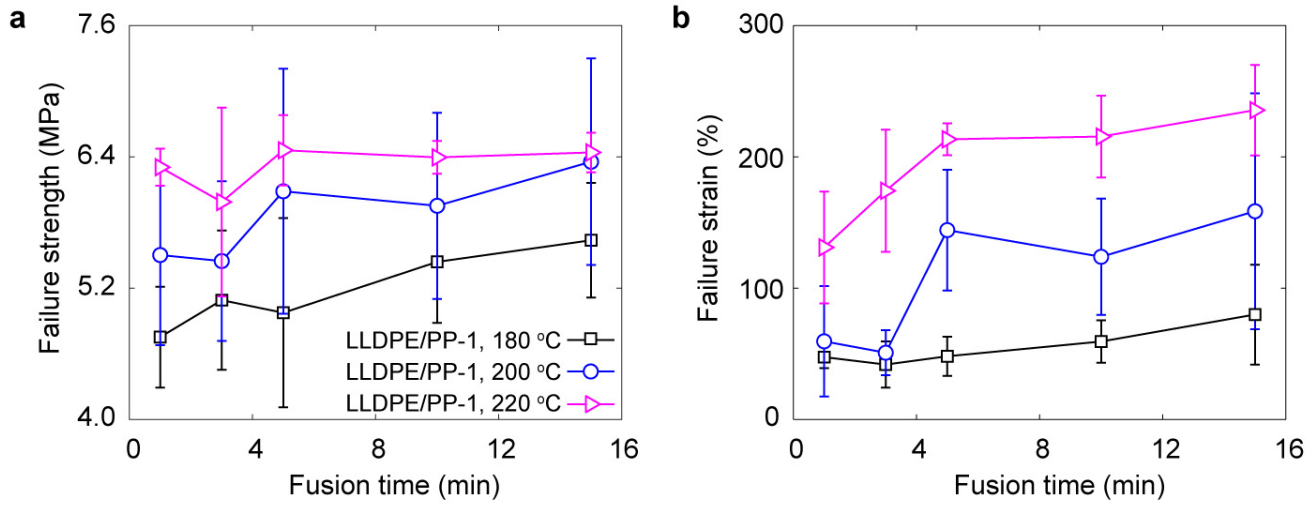

Figure S9. (**a**) The failure strength and (**b**) strain to failure of the LLDPE/PP-1 samples measured at different fusion temperature ($T = 180,\ 200,\ 220\ ^{o}$C).

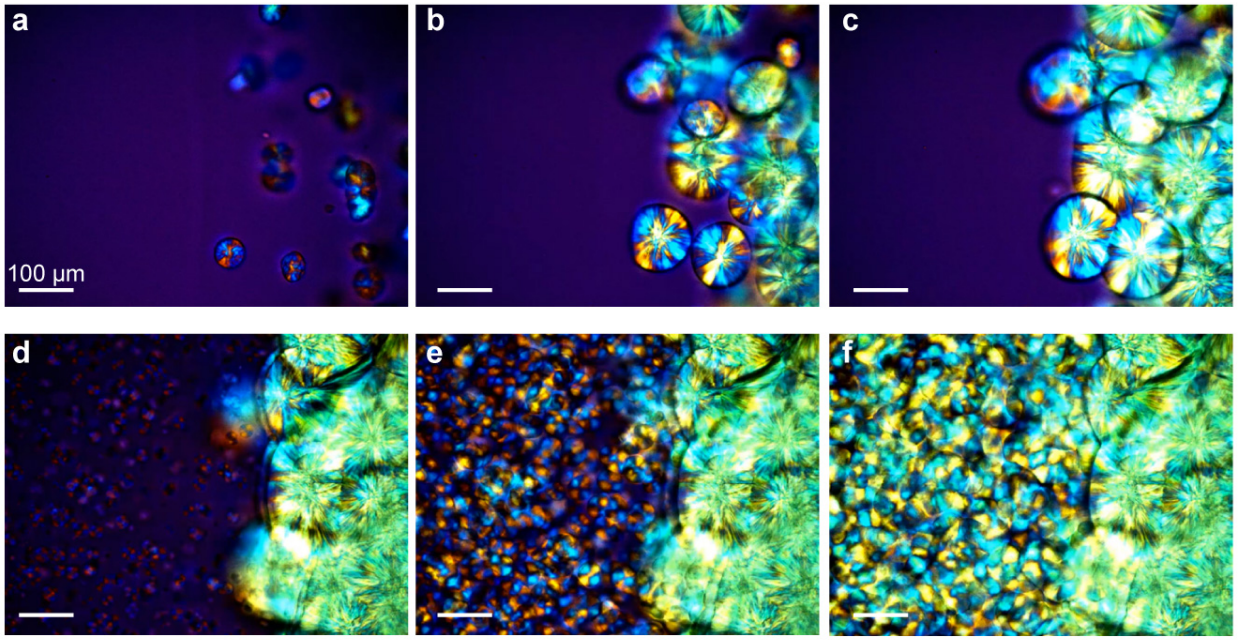

Figure S10. Isothermal crystallization at the LLDPE/PP-1 interfaces. Crystallizations of (**a**-**c**) PP-1 (right) at $\sim$ 130 °C and (**d**-**f**) LLDPE (left) at $\sim$ 110 °C. The crystallizations for LLDPE and PP-1 start separately, and the interface does not induce the nucleation process of LLDPE or PP-1, suggesting that the crystallization has a minor effect on the degree of fusion. The scale bar is 100 µm.